Inorganica Chimica Acta 512 (2020) 119924

Contents lists available at ScienceDirect

Inorganica Chimica Acta

journal homepage: www.elsevier.com/locate/ica

Research paper

Photocatalytic degradation of dyes by mononuclear copper(II) complexes from bis-(2-pyridylmethyl)amine NNN-derivative ligands

Samira S.F. Carvalho, Ana Carolina C. Rodrigues, Juliana F. Lima, Nakédia M.F. Carvalho*

Universidade do Estado do Rio de Janeiro, Instituto de Química, Rua São Francisco Xavier, 524, Edifício Haroldo Lisboa da Cunha, IQ, Room 312a, Maracanã, 20550-013 Rio de Janeiro, RJ, Brazil

ARTICLE INFO

Keywords:
Photo-Fenton
Copper(II) complexes
Methyl orange
Methylene blue
Crystal violet
Congo red
Rhodamine B
Dye degradation
Kinetics

ABSTRACT

Photocatalytic degradation of organic pollutant dyes under ultraviolet radiation has emerged as an efficient wastewater treatment. This work describes the application of four mononuclear copper(II) complexes coordinated to NNN ligands: bis-(2-pyridylmethyl)amine (BMPA), *N*-methylpropanoate-*N*,*N*-bis-(2-pyridylmethyl) amine (MPBMPA), *N*-propanoate-*N*,*N*-bis-(2-pyridylmethyl)amine (PBMPA) and *N*-propanamide-*N*,*N*-bis-(2-pyridylmethyl)amine (PABMPA); in the photocatalytic degradation of different dyes: methyl orange (MO), methylene blue (MB), crystal violet (CV), Congo red (CR) and Rhodamine B (RhB). The reactions were carried out under a UV lamp of 250 W, where 100% of degradation was achieved in 90 min for all complexes using hydrogen peroxide as oxidant. Kinetic experiments were carried out to investigate the photodegradation of the dyes under a UV lamp of 24 W. The reactions followed a zero-order model in relation to the dye, showing that its concentration did not play a significant role in the photocatalysis. The reaction order in relation to hydrogen peroxide varied from 0 to 0.8, from low to high concentrations of oxidant. The light intensity and the intrinsic catalytic activity of the complexes are the most important features for the dye photodegradation pathway.

1. Introduction

Environmental pollution caused by organic compounds is an important issue concerning the future well-being of the global society. The textile industry is responsible for 17–20% of the pollution caused by the discard of untreated wastewater into water bodies [1–3], representing a longstanding problem that causes environmental degradation, aesthetic issues, and toxicity to aquatic and human lives [4–5]. Dyes are complex and chemically stable molecules, design to last long, therefore resistant to harsh conditions such as sunlight, water, soap, bleach and perspiration. The conventional degradation methods are not always effective and can release traces of these compounds in rivers and lakes [4,6]. Apart of being non-biodegradable, dyes and its products can be carcinogenic, teratogenic and present acute toxicity [1], hence, new methodologies to treat these organic pollutants efficiently before disposal is mandatory for a cleaner and sustainable chemical industry.

Among the several biological, physical and chemical methods to mitigate the damage caused by the dyes, the Advanced Oxidation Processes (AOPs) have been highlighted [6]. For instance, Fenton and photo-Fenton systems rely on the use of safe and eco-friendly transition metal catalysts, traditionally iron(II) salts, and hydrogen peroxide to generate the highly oxidant hydroxyl radical that can mineralize a wide sort of organic pollutants of different structures and stability [7]. Nevertheless, compounds containing cobalt, manganese, ruthenium, cadmium, silver and copper have also been investigated as Fenton-like catalysts [6,8–11].

In the last decade, copper(II) complexes have been emerging as photo-Fenton catalysts for dye oxidative degradation. Complexes with salen-based ligand was tested in the photodegradation of Rhodamine B under visible light [12]. Copper(II) 1D and 3D frameworks with different ligands have been described in the degradation of different organic dyes under visible light irradiation [13–19]. Although a number of works have reported the efficiency of metal complexes for dye degradation, they are selective or studied for only one or two dyes. Furthermore, more detailed investigation about the mechanism of complex-mediated photocatalysis are still needed. Many publications described a first-order kinetics in relation to the dye, however, in many cases the data are not of good quality with very few points to assign reliably the correct kinetic model. Recent publication by Ollis [20] has shown that for heterogeneous photocatalysis the most suitable reaction model is zero-order in relation to the reactant, however, misinterpretation of the data has led many author to assign it as first-order.

Coordination compounds can absorb UV or visible light and assist catalytic process [15], what is advantageous for photo-Fenton system

* Corresponding author.
E-mail address: nakedia@uerj.br (N.M.F. Carvalho).

https://doi.org/10.1016/j.ica.2020.119924
Received 12 June 2020; Received in revised form 22 July 2020; Accepted 22 July 2020
Available online 25 July 2020

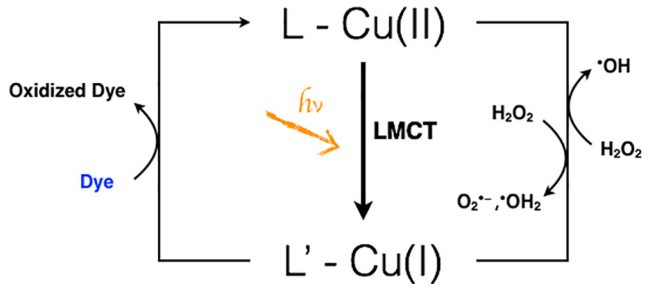

Fig. 1. Photo-Fenton mechanism for copper(II) complexes [17]. (LMCT: Ligand to Metal Charge Transfer. L = Ligand, L'= Oxidized Ligand).

because of the presence of both organic ligand and transition metal. Different ligand to metal charge transfers (LMCT) can occur and the oxidized metal species can also interact with H_2O_2 to form reactive oxygen or free radical species [16,17,21]. In the presence of UV or visible radiation Cu(II) complexes absorb photons leading to the formation of oxidized ligand (L') and Cu(I). The L' can interact directly with oxidizing pollutants (dyes), thereafter, regenerating the reduced ligand form (L). Copper(I) reacts with H_2O_2 to produce $^{\bullet}OH$ radicals. In parallel, independently of light irradiation, Cu(II) can react with H_2O_2 to generate $O_2^{\bullet-}$ and $^{\bullet}OH_2$. Fig. 1 simplifies the photo-Fenton mechanism of the catalyst based on copper(II) complexes. Other non-photoassisted charge transfer reactions can also be involved, for instance Cu(II) complexes can interact with peroxide to form intermediate species such as (L)Cu(II)–OOH or (L)Cu(I)-superoxide. The reactive species formed are strongly oxidizing and can degrade organic dyes. Furthermore, copper is stable in a larger range of pH compared to the traditional iron Fenton catalysts, and deactivation of the catalyst by hydroxide/oxide precipitation is less critical [17].

Metal transition coordination compounds with the versatile NNN ligand bis-(2-pyridylmethyl)amine (BMPA) have been applied in catalytic oxidation reactions [22,23]. The complex [Cu(BMPA)Cl_2] was successfully described as catalyst in the oxidation of cyclohexane with high conversions, using hydrogen peroxide as oxidant at mild conditions [24], being a promising catalyst for oxidative degradation of organic dyes as well. This work aims to investigate four mononuclear copper(II) complexes based on BMPA and derivative ligands: *N*-methylpropanoate-*N*,*N*-bis-(2-pyridylmethyl)amine (MPBMPA), *N*-propanoate-*N*,*N*-bis-(2-pyridylmethyl)amine (PBMPA) and *N*-propanamide-*N*,*N*-bis-(2-pyridylmethyl)amine (PABMPA), in the degradation of dyes of different structures by photo-Fenton, namely methyl orange (MO), methylene blue (MB), crystal violet (CV), Congo red (CR) and Rhodamine B (RhB). The studied ligands are strong Lewis bases and can favor the Cu(I)/Cu(II) redox cycle through LMCT, during the photocatalysis. Besides, ancillaries functional groups as carboxylate, methyl ester and amide, can tune the complex catalytic activity, and the unsaturated coordination of the proposed complexes can induce decomposition of hydrogen peroxide and enhance the catalytic performance [17]. Lastly, the kinetics of the dye photodegradation were investigated *in situ*, in order to provide information about the reaction mechanism.

2. Experimental

2.1. Materials and methods

All chemicals are of reagent grade and were used without further purification. Hydrogen peroxide (30% aqueous solution) from Sigma-Aldrich was titrated by the iodometric method and the determined concentration was 9.23 mol L^{-1}.

FTIR analyses were acquired in a Nicolet 6700, Thermo Scientific spectrophotometer, in KBr pellets for the complex characterization or as film over KBr window in the case of the ligands. The complexes were analyzed by ESI-(+)-MS/Q-TOF mass spectrometry in a MicrOTOF-Q II instrument from Bruker Daltonics, at capillary voltage of 4.0 kV in positive ion polarity, at 1.0×10^{-4} mol L^{-1} methanol:water solution. Conductimetric measurements of the complexes at 1.0×10^{-3} mol L^{-1} methanol solution were carried out in Gehaka CG 1800 instrument, with constant cell of 1.0 cm^{-1}. Complex characterization and dye degradation were acquired by solution UV–VIS spectroscopy, recorded on a diode-array Agilent 8453 spectrophotometer.

2.2. Synthesis of the complexes

The ligands BMPA, MPBMPA, PBMPA and PABMPA were synthesized according to published procedures [25,26], as shown in **Scheme S1**.

2.2.1. Complex [Cu(BMPA)Cl_2]

The complex dichloro[*bis*-(2-*pyridylmethyl*)*amine*]copper(II) was obtained following the published procedure [24]. A solution of the ligand BMPA (1.0 mmol; 0.199 g, in 5.0 cm^3 of ethanol) was added to a solution of $CuCl_2{\cdot}2H_2O$ (0.5 mmol, 0.852 g, in 5.0 cm^3 of ethanol) and a light blue precipitate was immediately obtained, which was filtered and washed with ethanol (41% of yield).

FTIR (KBr, cm^{-1}): 3436, 3068, 2910, 2890, 1606, 1573, 1481, 1435, 775. ESI-(+)-MS/Q-TOF: *m/z* 631.0008 $[Cu_2(BMPA)_2Cl_3]^+$, *m/z* 297.0184 $[Cu(BMPA)Cl]^+$, *m/z* 261.0393 $[Cu(BMPA)]^+$. UV–VIS (methanol, λ[nm] (ε[dm^3 mol^{-1} cm^{-1}])): 251 (8.9×10^3), 671 (1.1×10^2). Λ_M (methanol) = 88.4 Ω^{-1} cm^2 mol^{-1}.

2.2.2. Complex [Cu(MPBMPA)Cl](ClO_4)

The complex perchlorate of chloro[*N-methylpropanoate-N,N-bis*-(2-*pyridylmethyl*)*amine*]copper(II) was obtained by the addition of a solution of the ligand MPBMPA (0.88 mmol, 0.151 g, in 5.0 cm^3 of ethanol) to a solution of $CuCl_2{\cdot}2H_2O$ (1.76 mmol, 0.50 g, in 5.0 cm^3 of ethanol). The new solution was stirred for 30 min and no precipitate was formed. Then, 1.76 mmol of $NaClO_4$ was added (0.247 g), the solution was left to rest around 5 °C, after which a light blue precipitate was formed. The solid was filtered and washed with ethanol (41% of yield).

FTIR (KBr, cm^{-1}): 3443, 3079, 2955, 2923, 1711, 1612, 1447, 1283, 1105, 775. ESI-(+)-MS/Q-TOF: *m/z* 383.046 [Cu(MPBMPA)Cl]$^+$, *m/z* 348.0849 $[Cu(MPBMPA)]^+$. UV–VIS (methanol, λ[nm] (ε[dm^3 mol^{-1} cm^{-1}])): 257 (9.1×10^3), 678 (9.6×10^1). Λ_M (methanol) = 116.4 Ω^{-1} cm^2 mol^{-1}.

2.2.3. Complex [Cu(PBMPA)](ClO_4)

The complex perchlorate of [*N*-propanoate-*N*,*N*-bis-(2-pyridylmethyl)amine]copper(II) was obtained by the addition of a solution of the ligand PBMPA (1.0 mmol, 0.278 g, in 5.0 cm^3 of methanol) to a solution of $Cu(ClO_4)_2{\cdot}6H_2O$ (1.0 mmol, 0.371 g, in 5.0 cm^3 of methanol). The new mixture was stirred for 3 h and a blue precipitate was formed (79% of yield).

FTIR (KBr, cm^{-1}): 3430, 3088, 2923, 1612, 1572, 1500, 1441, 1316, 1092, 762. UV–VIS (methanol, λ[nm] (ε[dm^3 mol^{-1} cm^{-1}])): 263 (1.4×10^4), 690 (8.1×10^1). Λ_M (methanol) = 88.9 Ω^{-1} cm^2 mol^{-1}.

2.2.4. Complex [Cu(PABMPA)Cl]Cl

The complex chloride of chloro[*N-propanamide-N,N-bis*-(2-*pyridylmethyl*)*amine*]copper(II) was synthesized by the addition of a solution of the ligand PABMPA (1.0 mmol, 0.273 g, in 5.0 cm^3 of ethanol) to a solution of $CuCl_2{\cdot}2H_2O$ (1.0 mmol, 0.173 g, in 5.0 cm^3 of ethanol). The new mixture was stirred for 30 min and a light blue precipitate was formed (28% of yield).

FTIR (KBr, cm^{-1}): 3440, 3274, 3075, 3037, 2922, 1655, 1610, 1437, 765, 644. ESI-(+)-MS/Q-TOF: *m/z* 368.0616 [Cu(PABMPA)Cl]$^+$; *m/z* 356,1094 $[Cu(PABMPA)]^+$. UV–VIS (methanol, λ[nm] (ε[dm^3 mol^{-1} cm^{-1}])): 257 (9.2×10^3), 680 (8.9×10^1). Λ_M (methanol) = 174.4 Ω^{-1} cm^2 mol^{-1}.

2.3. Photo-Fenton dye degradation tests

Individual stock solutions of the dyes methyl orange (MO), methylene blue (MB), crystal violet (CV), Congo red (CR) and Rhodamine B (RhB), were prepared in distilled water at 5.0×10^{-4} mol L^{-1}.

In a typical experiment, 300 μL of aqueous 5.0×10^{-4} mol L^{-1} stock solution of a given dye, 200 μL of aqueous 5.0×10^{-4} mol L^{-1} complex stock solution, 10 μL of aqueous H_2O_2 9.23 mol L^{-1} stock solution and 2.49 mL of H_2O to complete a total reaction volume of 3.0 mL, were sequentially mixed in a glass capped vial. The resulting initial concentrations were: [dye] = 5.0×10^{-5} mol L^{-1}; [complex] = 3.3×10^{-5} mol L^{-1}; [H_2O_2] = 3.1×10^{-2} mol L^{-1}, resulting in 1:1.5:940 complex:dye:H_2O_2 molar ratio. The reaction was carried out under magnetic stirring, at 25 °C, and at preset time intervals UV–VIS spectra were collected. To maintain the homogeneity in the photon flux distribution [27], a vapor Hg lamp (250 W) to simulate UV radiation was fixed 25 cm from the sample (**Scheme S3(A)**). Control tests were performed with no light irradiation to confirm that the complexes do not have any catalytic effect in the dark.

To determine the reaction order in relation to dye and hydrogen peroxide, initial concentration was varied separately: 100 – 300 μL of aqueous 5.0×10^{-4} mol L^{-1} stock solution of methyl orange: [MO] = 1.7×10^{-5} – 5.0×10^{-5} mol L^{-1}; 10 – 500 μL of aqueous H_2O_2 9.23 mol L^{-1} stock solution: [H_2O_2] = 3.1×10^{-2} – 1.5 mol L^{-1}.

The experiment was set up to allow the kinetic investigation and simultaneous collection of UV–VIS data, therefore mild conditions such as distance and potency of the light source were employed recombined. The kinetic experiments were conducted in a capped cuvette inside the UV–VIS spectrometer by *in situ* photocatalysis conducted under UV light (external Black light 24 W from Philips) fixed 12 cm from the cuvette, under stirring at 25 °C (**Scheme S3(B)**). Both photocatalytic system was kept closed by a physical barrier to avoid dissipation and leakage of harmful light. The lamp of the spectrophotometer was turned on only during the electronic spectrum acquisition.

The MO decolorization was calculated using the following equation:

$$Degradation\,(\%) = \left[\frac{Abs_0 - Abs_t}{Abs_0}\right] \times 100 \quad (1)$$

3. Results and discussion

3.1. Characterization of the complexes

Four mononuclear copper(II) complexes were synthesized (**Scheme S2**) and characterized by FTIR, electronic spectroscopy in UV–VIS region, ESI-(+)-MS/Q-TOF and conductimetry, as presented in the Supporting Information. The proposed structures are presented in Fig. 2.

The complex [Cu(BMPA)Cl_2] adopts a five-coordinated distorted square-pyramidal geometry, with one elongated Cu-Cl bond, according to published single crystal X-ray structure [28,29]. Relatively high electric conductivity (**Table S1**) for a neutral complex confirms the lability and week coordination of the chloride ligand [30]. ESI-(+)-MS/Q-TOF spectrum (**Fig. S5**) shows peaks related to dimeric species in solution $[Cu_2(BMPA)_2Cl_3]^+$ at *m/z* 631.0008 and to monomeric species $[Cu(BMPA)Cl]^+$ at *m/z* 297.0184.

In the synthesis of [Cu(MPBMPA)Cl](ClO_4) the counter-ion perchlorate was necessary to form a precipitate, ionic ClO_4^- was confirmed by the FTIR large band at 1093 cm^{-1} (**Fig. S2**) and by the electrical conductivity typical of a 1:1 electrolyte (**Table S1**) [30]. The FTIR band of the ester group can provide information about the coordination to the copper(II) center, where a negative shift of the carbonyl stretching frequency and a positive shift of the C—O stretching frequency have been taken as evidence for the carbonyl oxygen acting as donor atom [31]. In the free ligand MPBMPA, C═O appears at 1737 cm^{-1} and C—O at 1243 cm^{-1}, while in the complex these bands appear at 1711 and 1283 cm^{-1}, respectively, what can suggest that the methyl ester group is interacting weakly with the copper(II) center. Therefore, it is proposed a cationic five coordinated complex with one chloride ligand coordinated to the copper(II) center. This proposed structure is different from the published single crystal X-ray data for [Cu(MPBMPA)Cl_2], which adopted a square pyramidal geometry and presented two chloride ions as ligands. Besides, it presented an unchanged $\nu(CO_2)_{as}$ at 1731 cm^{-1} in relation to the free ligand, since the ester group appears uncoordinated [32]. The structure is also confirmed by the species $[Cu(MPBMPA)Cl]^+$ at *m/z* 383.046 in the ESI-(+)-MS/Q-TOF spectrum (**Fig. S6**).

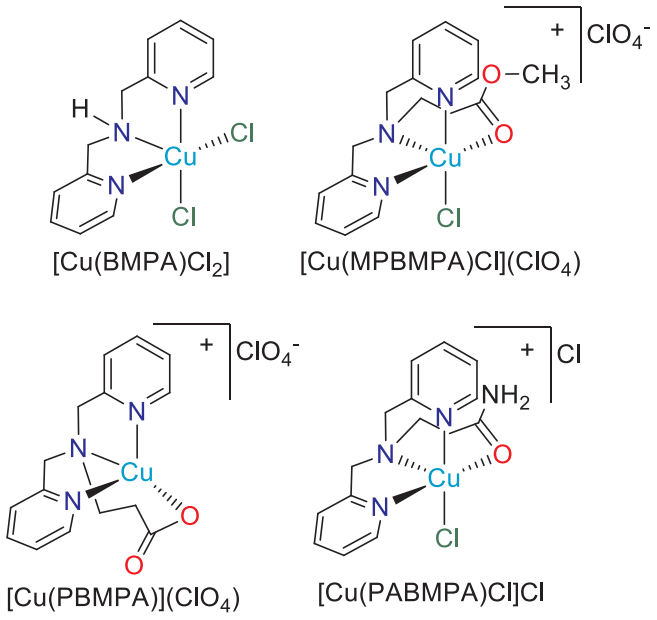

Fig. 2. Proposed structures of the copper(II) complexes.

Complex [Cu(PBMPA)](ClO_4) was prepared with $Cu(ClO_4)_2$ since no product was obtained from the synthesis with $CuCl_2$, ionic ClO_4^- was confirmed at 1092 cm^{-1} (**Fig. S3**) and by the electrical conductivity typical of 1:1 electrolyte. The carboxylate $\nu(CO_2)_{as}$ and $\nu(CO_2)_s$ bands can give information about the coordination mode to the copper(II) center. In the free ionic ligand the bands appear at 1597 and 1384 cm^{-1}, resulting in $\Delta\nu(CO_2)$ = 213 cm^{-1}. In the complex a higher value for $\Delta\nu(CO_2)$ = 1645 − 1311 = 334 cm^{-1} indicates a monodentate coordination mode [33]. The similar complex [Cu(PBMPA)Cl] showed a pentacoordinated square pyramidal geometry, with the chloride ion coordinated to copper(II) [32]. In the present synthesis, a solvent molecule could be occupying the fifth position of the coordination sphere.

Finally, for the complex [Cu(PABMPA)Cl]Cl it is proposed as a five coordinated structure, with the coordination of the amide oxygen to the copper center. This is confirmed by the amide C═O band shift from 1677 in the free ligand to 1650 cm^{-1} in the complex (**Fig. S4**). The electrical conductivity is compatible with a 2:1 electrolyte, probably due to the lability of the chloride ion. Similar coordination mode was observed for the iron(III) complex [Fe(PABMPA)Cl_2](ClO_4) with the C═O band at 1653 cm^{-1} [25], and for the copper(II) complex with the analogous ligand *N*-alanineamide-*N*,*N*-bis-(2-pyridylmethyl)amine (dpgs) [Cu(dpgs)Cl]ClO_4 that also presented square pyramidal geometry with coordination by the amide oxygen [34].

For all complexes (**Figs. S1–S4**, **Table S2**), electronic UV–VIS spectra showed three major bands: a stronger band around 270 nm assigned to π → π* intraligand charge transfer, a band centered at 300 nm assigned to metal-to-ligand charge transfer, and a weaker band

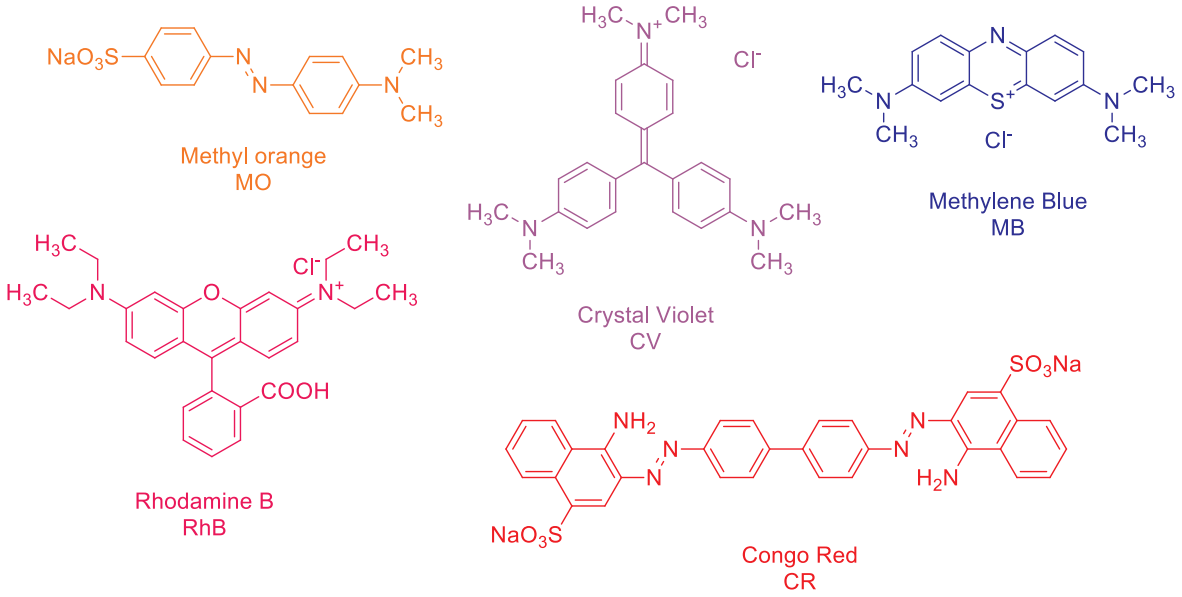

Fig. 3. Structure of the studied dyes.

around 670 nm from d-d transition.

3.2. Photo-Fenton dye degradation tests

The mononuclear Cu(II) complexes prepared were investigated as catalysts in the photodegradation of five dyes of different structures: methyl orange (MO), methylene blue (MB), crystal violet (CV), Congo red (CR) and Rhodamine B (RhB) (Fig. 3). The reactions were carried out in water, due to the high solubility of the complexes, at 1:1.5:940 of complex:dye:H_2O_2 molar ratio, at 25 °C, in a homemade photocatalytic reactor equipped with UV lamp (250 W) (**Scheme S3**).

Initially, the influence of the presence of UV light, H_2O_2 and catalyst on dye degradation was evaluated. The tests were carried out using [Cu(MPBMPA)Cl](ClO_4) as catalyst and methyl orange as dye. Also, $CuCl_2$ and pure ligand MPBMPA (L) were tested to study the impact of free Cu (II) ions and free ligand on the photocatalysis.

Fig. 4**(a)** shows that the photodegradation reaction only induced by UV light without catalyst or H_2O_2, does not lead to the degradation process within the studied reaction time. Posteriorly, the catalyst was added to the medium and no change was observed. Therefore, the following tests were performed with H_2O_2 and three new systems were evaluated. Firstly, the degradation test was performed only in the presence of catalyst and H_2O_2 under dark and the dye absorbance spectrum did not show any evidence of degradation. A test was also carried out by adding only H_2O_2 into the reaction medium and submitting the system to UV irradiation and 38% of dye degradation was observed after 90 min, due to light induced formation of reactive oxygen species responsible for the dye degradation. Finally, the system composed by catalyst, H_2O_2 and UV light was evaluated and the system allowed a total photodegradation of methyl orange, revealing a promising result and the effect of the catalyst in the photodegradation. The results are summarized in Table 1.

In order to understand the effect of pure Cu(II) ions and free ligand in the reported homogeneous photocatalysis, the previous system was repeated either replacing [Cu(MPBMPA)Cl](ClO_4) by a Cu(II) salt, $CuCl_2$, or by the free ligand MPBMPA. The system containing only ligand, H_2O_2 and UV reached a degradation of 76% of MO. Considering that the reaction medium contains reactive oxygen species such as $^{\bullet}OH$, from the H_2O_2 photolysis induced by UV irradiation, the ligand can be oxidized by these species or by photon absorption and the oxidized ligand can interact directly with MO improving dye degradation. Furthermore, the system formed by only Cu(II) salt, H_2O_2 and UV light showed 100% of degradation, indicating that the photodegradation of the dye is also catalyzed by the copper(II) salt. In addition to the performance of the radicals generated by H_2O_2 + UV, Cu(II) ions also react with H_2O_2 forming $^{\bullet}OH$, $O_2^{\bullet-}$ and $^{\bullet}OH_2$ [17].

The system formed by Cu(II) salt + ligand + H_2O_2 + UV was also evaluated and MO degradation of 98% was achieved. In comparison to the isolated complex [Cu(MPBMPA)Cl](ClO_4) + H_2O_2 + UV that also showed 100% of MO degradation, when Cu(II) and ligand are mixed *in situ* they can interact readily and allow LMCT to take place. These results indicate that either isolated complex or *in situ* formed complex can contribute to the photocatalysis and act efficiently in the degradation of the studied pollutants. Although both complex and salt lead to 100% of

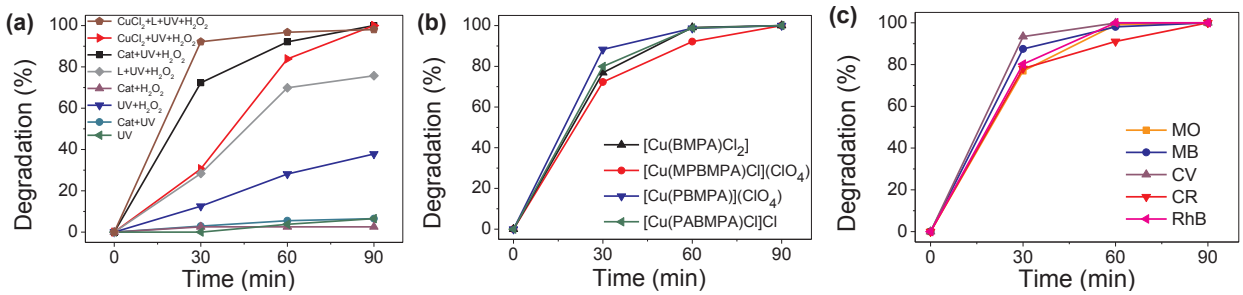

Fig. 4. Photodegradation of methyl orange at complex:dye:H_2O_2 molar ratio of 1:1.5:940, 25 °C, UV light (250 W): (a) in different conditions with [Cu(MPBMPA)Cl](ClO_4) as catalyst; (b) by different Cu(II) complexes; (c) of different dyes by [Cu(BMPA)Cl_2] as catalyst. (For interpretation of the references to colour in this figure legend, the reader is referred to the web version of this article.)

Table 1
Photodegradation percentage of methyl orange at 90 min catalyzed by [Cu(MPBMPA)Cl](ClO$_4$).

Conditions[a]	Degradation$_{90min}$ (%)
UV	6.5
UV + H_2O_2	38
Catalyst + UV	6.5
Catalyst + H_2O_2	2.5
Catalyst + UV + H_2O_2	100
$CuCl_2$ + UV + H_2O_2	100
Ligand + UV + H_2O_2	76
$CuCl_2$ + Ligand + UV + H_2O_2	98

[a] MO at 5.0 × 10^{-5} mol L^{-1}; Catalyst: [Cu(MPBMPA)Cl](ClO$_4$) at 3.3 × 10^{-5} mol L^{-1}; H_2O_2 at 3.1 × 10^{-2} mol L^{-1} and UV light (250 W); Ligand: MPBMPA at 3.3 × 10^{-5} mol L^{-1}.

MO photodegradation after 90 min, Fig. 4**(a)** indicates that the photocatalysis in the presence of [Cu(MPBMPA)Cl](ClO$_4$) or $CuCl_2$ + MPBMPA allow higher rate of photodegradation. After few minutes, for [Cu(MPBMPA)Cl](ClO$_4$) and Cu(II) + Ligand photodegradation higher than 50% was reached, favored by the LMCT. Kinetic studies reported below enable full discussions.

Fig. 4**(b)** shows the results of MO degradation for all four Cu(II) complexes reported, which presented good photodegradation ability with complete degradation of the dye within 90 min. For [Cu(BMPA)Cl$_2$], [Cu(PBMPA)](ClO$_4$) and [Cu(PABMPA)Cl]Cl, 100% of MO is already decomposed in 60 min of irradiation.

In order to prove the efficiency of the copper(II) complexes in the photocatalysis of different dyes, the catalyst [Cu(BMPA)Cl$_2$] was employed (Fig. 4**(c)**). MO, MB, CV and RB dyes suffered total degradation after 60 min, however, for CR 90 min were necessary to achieve total degradation, probably because of the presence of two azo bonds and higher molecular weight. These results show the wide range of performance of the copper(II) complexes, degrading dyes with different structures and classes.

3.3. Kinetic experiments of dye photodegradation

In order to get information about the reaction mechanism of the dye photodegradation, kinetic experiments were carried out in water, at 25 °C. To set up an experiment where UV–VIS spectra were recorded at every 1 min for 90 min, an UV lamp of lower intensity (24 W) was coupled to the spectrophotometer allowing the cuvette to be irradiated during the whole reaction time (**Scheme S3(B)**).

Fig. 5**(a)** shows typical UV–VIS spectra acquired during the degradation of the azo dye methyl orange, catalyzed by [Cu(BMPA)Cl$_2$], with H_2O_2 at 15.4 × 10^{-1} mol L^{-1} (1:1.5:45000 of complex:dye:H_2O_2 molar ratio). The band at λ_{max} = 464 nm is assigned to the azo bond. After addition of catalyst and H_2O_2, a considerable red-shift to λ_{max} = 495 nm was observed, suggesting subtle structural changes in MO probably due to interaction with the Cu(II) complex. The decay of the azo band over time indicates the destruction of the chromophore by the cleavage of the azo bond and disruption of conjugated π-bonds in the molecule, leading to colorless oxidized products [4,6].

Table 2
Degradation percentage and kinetic data of photodegradation of dyes.[a]

Catalyst	Dye	[H_2O_2] (mol L^{-1})	Degradation$_{90min}$(%)	k_{obs}(μmol L^{-1} min^{-1})[b]
[Cu(BMPA)Cl$_2$]	MO	0.031	45	0.274
	MO	0.062	51	0.286
	MO	0.154	67	0.425
	MO	0.31	79	0.561
	MO	0.37	100	1.106
	MO	0.46	100	1.311
	MO	0.62	95	1.256
	MO	0.92	96	1.735
	MO	1.23	99	1.894
	MO	1.54	98	2.565
[Cu(MPBMPA)Cl$_2$]	MO	1.54	100	2.962
[Cu(PBMPA)] (ClO$_4$)	MO	1.54	90	2.630
[Cu(PABMPA)Cl] Cl	MO	1.54	96	2.835
[Cu(BMPA)Cl$_2$]	CV	1.54	100	3.969
[Cu(BMPA)Cl$_2$]	RhB	1.54	100	7.012
[Cu(BMPA)Cl$_2$]	CR	1.54	88	0.201
[Cu(BMPA)Cl$_2$]	MB	1.54	100	3.933

[a] Catalyst at 3.3 × 10^{-5} mol L^{-1}; dye at 5.0 × 10^{-5} mol L^{-1}; UV light (24 W).
[b] Zero-order rate constant.

Fig. 5**(b)** shows the time trace for the decay of MO absorbance at λ_{max} = 495 nm, for different concentrations of H_2O_2. In a first moment, experiments catalyzed by [Cu(BMPA)Cl$_2$] were carried out using the same H_2O_2 concentration as with the vapor Hg lamp (0.031 mol L^{-1}), however, only 45% of degradation was achieved in 90 min due to the lower radiation intensity of the 24 W lamp. So, the H_2O_2 concentration was increased until complete degradation was achieved, as summarized in Table 2.

Concerning the kinetic study of the photodegradation, eq. (2) shows a proposed rate law for the reaction.

$$-\frac{d[dye]}{dt} = v = k[dye]^a[H_2O_2]^b \quad (2)$$

At excess of H_2O_2, the equation can be simplified and the effect of the dye concentration in the reaction rate can be isolated (eq. (3) and (4)).

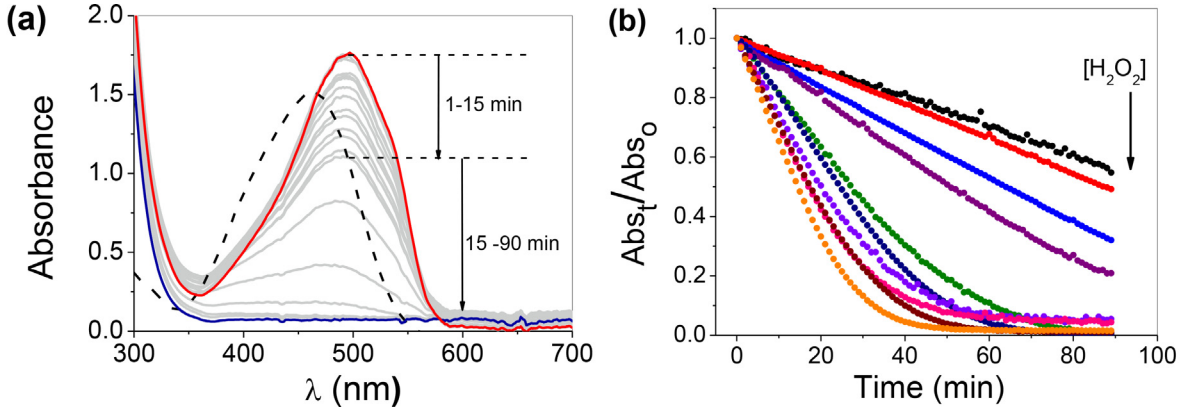

Fig. 5. (a) UV–VIS spectra of **MO** photodegradation by [Cu(BMPA)Cl$_2$], H_2O_2 and UV light (24 W). Dashed line: pure MO. (b) Time trace at λ_{max} = 495 nm at different concentrations of H_2O_2 from 0.031 to 1.54 mol L^{-1} (see Table 2).

$$-\frac{d[dye]}{dt} = v = k_{obs}[dye]^a \quad (3)$$

where,

$$k_{obs} = k[H_2O_2]^b \quad (4)$$

As shown in Fig. 5**(b)**, at lower concentrations of oxidant, but still at large excess in relation to the dye, it is clear by the shape of the curve that the kinetics follows pseudo-zero order equation (eq. (5) and (6)), where the concentration of the dye over time did not affect the reaction rate.

$$-\frac{d[dye]_t}{dt} = k_{obs} \quad (5)$$

$$[dye]_t = -k_{obs}t \quad (6)$$

To confirm the reaction order in relation to the dye, the MO absorbance decay with time was fit by the integrated equations for the most common reaction orders: zero-, first- (eq. S1 - S2) and second-order (eq. S3). Fig. 6**(a)** shows the fitting for the lowest H_2O_2 concentration tested (0.031 mol L^{-1}), where the R^2 is high for both zero- and first-order. Fig. 6**(b)** shows the linear plot for first-order, where the linear regression R^2 is also reliable, although a deviation from the experimental data and a parabolic residual plot (**Fig. S9**) indicates that this is not the most appropriated model to describe the system. The same behavior was observed for the concentrations from 0.031 to 0.31 mol L^{-1} (**Figs. S9 – S12**). However, as the concentration of H_2O_2 further increased **(Figs. S13–S18)**, it is less evident that the data still follows a zero-order model, as can be seen for the highest H_2O_2 concentration tested in Fig. 7**(a)**. After 40 min the dye was completely consumed, and the shape of the curve could be misinterpreted as an exponential decay of first-order reaction, but the linear plot (Fig. 7**(b)**) undoubtedly rules out the first-order model. In the high H_2O_2 concentration cases, to find the zero-order kinetic constant rate, the data was fitted only in the beginning of the reaction.

To provide further evidence of the reaction order, in a second set of experiments the initial concentration of methyl orange was varied as shown in Fig. 8**(a)**. The **Figs. S19–S23** show the fits for all MO concentrations tested. Table 3 presents the values of the observed pseudo-zero order rate constants and Fig. 8**(b)** presents the log plot of k_{obs} versus MO concentration. Although a variation was observed in the values from experimental error, an horizontal straight line with slope of 0.0015 confirms the assigned pseudo-zero order in relation to MO.

Ollis [20] have established based on experimental kinetic data, that for heterogeneous photocatalysis the most suitable reaction model in relation to the reactant is zero-order. However, misinterpretation of the data has led many author to assign it as first-order, because the semilog plot of $C(t)$ vs. time is usually linear. However, they often exhibit apparent first-order rate constants that diminish with increasing reactant concentration, what is an evidence of the wrong assignment. Ollis showed that such studies are the result of intrinsic zero-order data plotted on a semilog graph, and involves zero-order rate limitation by reactant saturation, electron transfer to O_2, oxygen mass transfer, or light supply. Besides, the competition for oxidant between the dye and its oxidized intermediates, would exhibit an apparent first-order behavior over time, even while the initial rate is zero-order within the concentration range studied.

In the presented results of homogeneous catalysis, a similar behavior is taking place. The apparent first-order rate constants calculated from the exponential fit of the experimental data are expressed in **Table S3** and also diminish linearly with increased initial concentration of MO (**Fig. S24**), therefore, this is further confirmation that the reaction does not follow 1st-order mechanism, but a disguised zero-order behavior [20]. Silver(I) complexes at heterogeneous photodegradation condition also presented zero-order kinetics [35].

In order to determine the reaction order b in relation to H_2O_2 according to eq. (4), the plot k_{obs} versus $[H_2O_2]$ is shown in Fig. 9**(a)**, and a linear relation is expected if b is 1. A slight deviation for the first-order model was observed since the linear regression gives a relatively poor R^2 value of 0.937. The calculated average intrinsic first-order rate constant k is 1.464 min^{-1}. To confirm the reaction order in relation to H_2O_2, the logarithm was applied in both sides of eq. (6), leading to the relation represented in eq. (7).

$$log(k_{obs}) = log(k) + b.\ log([H_2O_2]_0) \quad (7)$$

Fig. 9**(b)** shows the plot of $\log(k_{obs})$ versus $\log([H_2O_2]_0)$ where it is clear that two different values of reaction order were observed for b: 0 at low H_2O_2 concentrations and 0.8 at high H_2O_2 concentrations. Probably at lower concentration of oxidant the light intensity plays the dominant role in the dye photodegradation, but at higher concentrations of oxidant the reaction rate is affected by its concentration. This may be due to the catalase-like activity displayed by the complex, that at low concentration of oxidant does not form enough hydroxyl radicals. However, at higher concentration of H_2O_2, the formation of hydroxyl radicals starts to play an important effect in the reaction rate. Evidence of catalase-like activity can be seen from the significant intercept in Fig. 9**(a)**, which has been associated with the parallel reaction of H_2O_2 disproportionation [37].

Fig. 10**(a)** compares the quenching of the azo band by the different copper(II) complexes, where [Cu(MPBMPA)Cl_2] was the most efficient with 100% of degradation and k_{obs} = 2.962 μmol L^{-1} min^{-1}, followed closely by [Cu(PABMPA)Cl]Cl k_{obs} = 2.835 μmol L^{-1} min^{-1} (**Figs. S25-S27**). [Cu(BMPA)Cl_2] and [Cu(PBMPA)](ClO_4) presented slightly smaller rate constants, 2.565 and 2.630 μmol L^{-1} min^{-1}, respectively. Intrinsic rate constants (Table 2) reflect the high catalytic activity of the

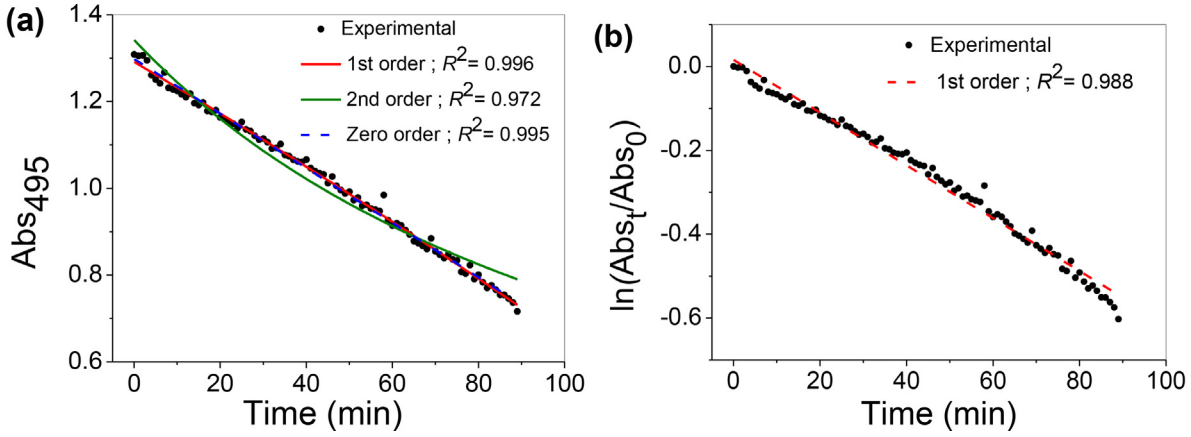

Fig. 6. (a) Kinetic fit of the time trace and linear plots of the UV–VIS band at λ_{max} = 495 nm, from the degradation of **MO** by **[Cu(BMPA)Cl_2]**, H_2O_2 (3.1 × 10^{-2} mol L^{-1}) and UV light (24 W). (b) Linear plot for first-order equation (**eq. S2**).

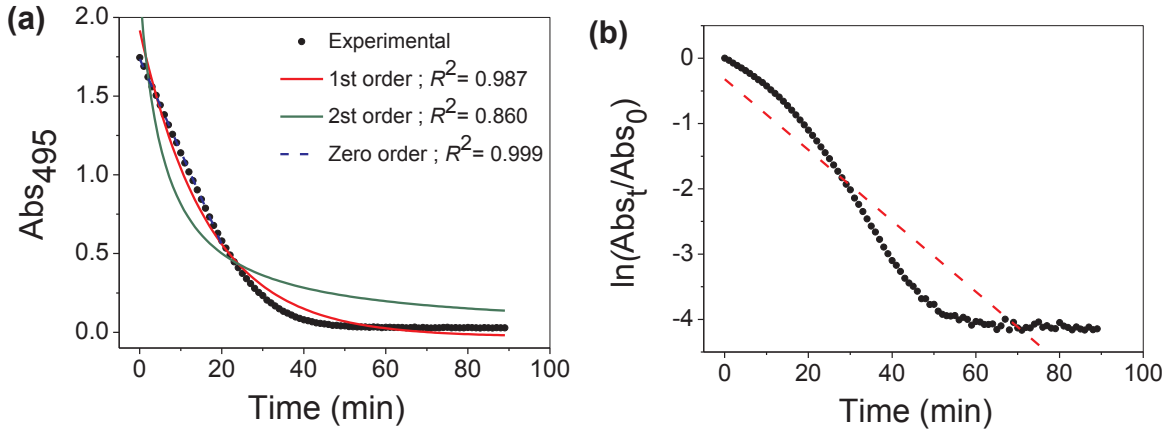

Fig. 7. (a) Kinetic fit of the time trace and linear plots of the UV–VIS band at λ_{max} = 495 nm, from the degradation of **MO** by **[Cu(BMPA)Cl$_2$]**, H_2O_2 (15.4 × 10^{-1} mol L^{-1}) and UV light (24 W). (b) Linear plot for first-order equation (**eq. S2**).

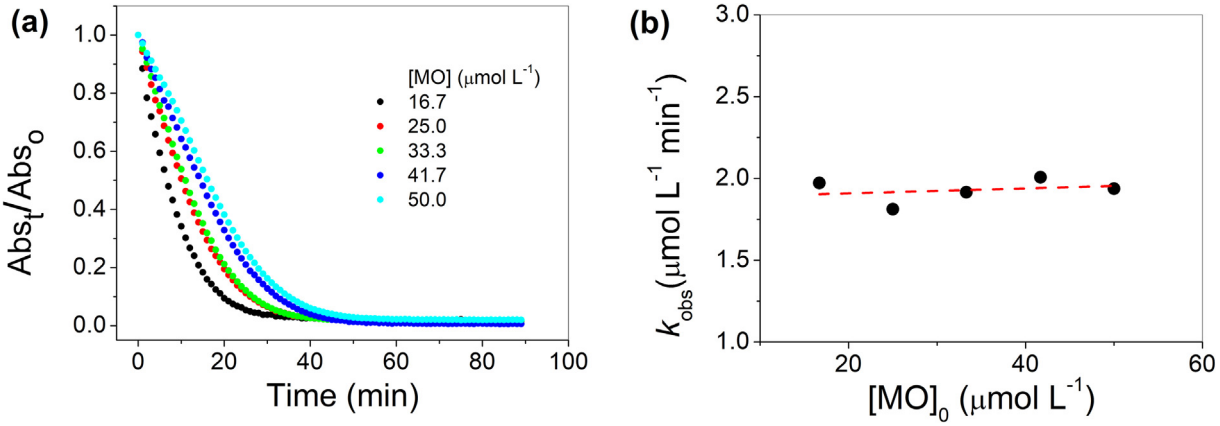

Fig. 8. (a) Time trace at λ_{max} = 495 nm for different initial concentration of MO and (b) respective log plot (**eq. (5)**), from the photo-degradation of **MO** by **[Cu(BMPA)Cl$_2$]** (3.3 × 10^{-5} mol L^{-1}), H_2O_2 (15.4 × 10^{-1} mol L^{-1}) and UV light (24 W).

Table 3
Degradation percentage and kinetic data of photodegradation of dyes.[a]

[MO]$_o$ (μmol L^{-1})	k_{obs} (μmol L^{-1} min^{-1})[b]
16.7	1.973
25.0	1.812
33.3	1.916
41.7	2.007
50.0	1.938

[a] Catalyst at 3.3 × 10^{-5} mol L^{-1}; dye at 5.0 × 10^{-5} mol L^{-1}; UV light (24 W).
[b] Zero-order rate constant.

complexes. Since all of them presented similar structures, ligands and charge transfers, similar behavior is expected. A correlation with redox potentials measured in DMSO for related iron(III) complexes with the same ligands showed that the complexes with the ligands MPBMPA and PABMPA presented the lowest redox potentials [36], what can favor the LMCT and consequently promoted the photocatalysis. By other side, the iron(III) complexes with BMPA and PBMPA presented the most negative redox potentials and more energy will be necessary to perform the LMCT.

Fig. 10**(b)** shows the degradation of the different dyes with the complex [Cu(BMPA)Cl$_2$], were it is possible to observe a complete decomposition at 50 min, except for Congo red (CR) that achieved 88% of degradation only after 90 min. According to the literature, the structure of the dye does not affect appreciably the photocatalytic reaction rate, but it is rather affected by the type of catalyst expressed in the rate constant *k*, and the hydroxyl radical concentration in the case of liquid-phase homogeneous catalysis, which is dependent of the intensity of the light [20]. The kinetic data were also well adjusted to zero-order for all dyes (**Figs. S28-S31**). This may be the case of the studied dyes, which presented similar values for zero-order k_{obs} (Table 2): MO: k_{obs} = 2.565, CV: k_{obs} = 3.969; MB: k_{obs} = 3.933 μmol L^{-1} min^{-1}. In the case of CR, two azo bonds are present and the k_{obs} = 0.201 μmol L^{-1} min^{-1} is roughly thirteen folds lower than the analogous MO that presented only one azo bond. By other side, the dye RhB presented a higher k_{obs} = 7.012 μmol L^{-1} min^{-1} probably because of its fluorescent property that favor the light absorption and subsequent degradation by the catalyst. Comparing with the data at the higher intensity vapor Hg lamp (250 W), the structure of the dye did not present any effect on the photocatalytic activity. But in the case of the lower intensity UV lamp (24 W), probably not enough OH· radicals were formed to degrade the two azo bonds of CR in 50 min.

4. Conclusions

Herein, the photocatalytic degradation of dyes of different structures: methyl orange, methylene blue, crystal violet, Congo red and Rhodamine B, promoted by copper(II) complexes with NNN derivative ligands was investigated. All dyes were successfully degraded in less than 90 min, under UV radiation provided by a vapor Hg lamp of 250 W, only in the presence of both complex and hydrogen peroxide as oxidant. The ligand to metal charge transfer (LMCT) was associated with the improvement in the catalytic degradation promoted by the complexes, enhancing even further the dye degradation by oxygenated

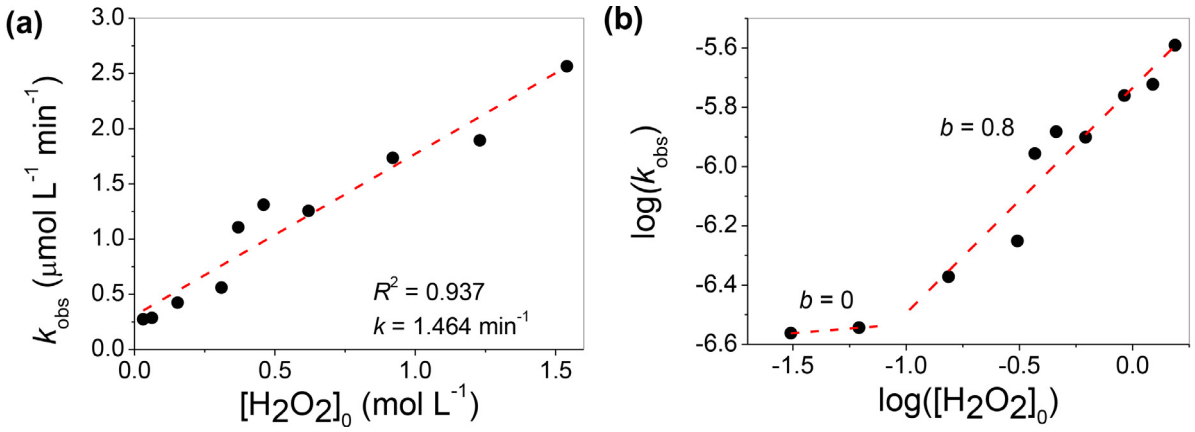

Fig. 9. (a) Zero-order rate constant versus H_2O_2 concentration (**eq.** (4)) and (b) respective log plot (**eq.** (7)), from the degradation of **MO** by **[Cu(BMPA)Cl$_2$]** and UV light (24 W).

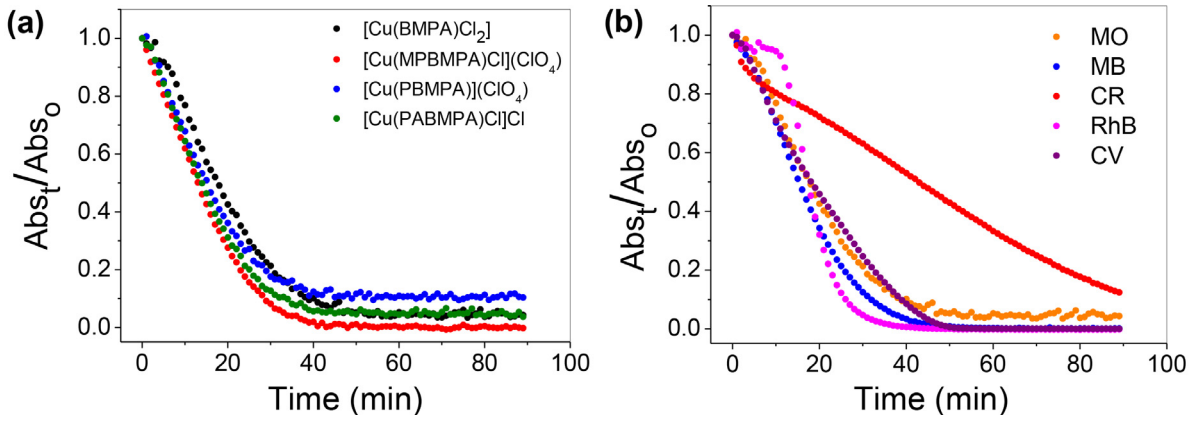

Fig. 10. (a) Time trace at λ_{max} = 495 nm for **MO** photo-degradation by different complexes, H_2O_2 (15.4 × 10^{-1} mol L^{-1}) and UV light (24 W). (b) Photo-degradation of different dyes catalyzed by [Cu(BMPA)Cl$_2$].

radials formed from Cu(II) ion, H_2O_2 and UV light. Kinetics experiments carried out *in situ* with a UV light of lower radiation, unveiled an unusual zero-order reaction in relation to the dye. The experimental data were better fit by a zero-order equation and experiments with variable initial concentration of dye showed that the zero-order rate constant did not vary with concentration, supporting this proposal. These results represent a new analysis of the kinetics of homogeneous photocatalysis of organic dyes, in accordance with described analogous heterogeneous photocatalysis. Moreover, a variable reaction order in relation to hydrogen peroxide was observed, from 0 to 0.8 from low to high concentrations of oxidant. It was also demonstrated that the effect of the light and type of catalysts together with the charge transfer that occurs between the metal and the ligands, plays the major role in determining the path of the dye photodegradation.

CRediT authorship contribution statement

Samira S.F. Carvalho: Data curation, Formal analysis, Investigation, Methodology, Validation. **Ana Carolina C. Rodrigues:** Data curation, Formal analysis, Methodology. **Juliana F. Lima:** Conceptualization, Formal analysis, Investigation, Methodology, Writing - original draft, Writing - review & editing. **Nakédia M.F. Carvalho:** Conceptualization, Formal analysis, Funding acquisition, Investigation, Methodology, Project administration, Resources, Supervision, Validation, Visualization, Writing - original draft, Writing - review & editing.

Declaration of Competing Interest

The authors declare that they have no known competing financial interests or personal relationships that could have appeared to influence the work reported in this paper.

Acknowledgements

We acknowledge Conselho Nacional de Desenvolvimento Científico e Tecnológico (BR) – CNPq (PQ-2/2018), Fundação de Amparo à Pesquisa do Estado do Rio de Janeiro – FAPERJ (JCNE 2018: E-26/203.023/2018) and Coordenação de Aperfeiçoamento de Pessoal de Nível Superior – Brasil (CAPES) (PROAP and PhD Scholarship) for supporting this project.

Appendix A. Supplementary data

Supplementary data to this article can be found online at https://doi.org/10.1016/j.ica.2020.119924.

References

[1] V. Katheresan, J. Kansedo, S.Y. Lau, J. Environ. Chem. Eng. 6 (2018) 4676–4697, https://doi.org/10.1016/j.jece.2018.06.060.
[2] T. Robinson, G. McMullan, R. Marchant, P. Nigam, Bioresour. Technol. 77 (2001) 247–255, https://doi.org/10.1016/S0960-8524(00)00080-8.
[3] C.-H. Wu, J.-M. Chern, Ind. Eng. Chem. Res. 45 (2006) 6450–6457, https://doi.org/10.1021/ie0602759.
[4] N. Chahbane, D.-L. Popescu, D.A. Mitchell, A. Chanda, D. Lenoir, A.D. Ryabov, K.-W. Schramm, T.J. Collins, Green Chem. 9 (2007) 49–57, https://doi.org/10.1039/

b604990g.
[5] E. Forgacs, T. Cserhati, G. Oros, Environ. Int. 30 (2004) 953–971, https://doi.org/10.1016/j.envint.2004.02.001.
[6] Y.-B. Lu, C.-H. Wang, H.-J. Du, Y.-Y. Niu, Inorg. Chim. Acta 450 (2016) 154–161, https://doi.org/10.1016/j.ica.2016.05.039.
[7] A. Colombo, C. Dragonetti, M. Magni, D. Roberto, Inorg. Chim. Acta 431 (2015) 48–60, https://doi.org/10.1016/j.ica.2014.12.015.
[8] Y.-J. Wu, D.-C. Hu, X.-Q. Yao, Y.-X. Yang, J.-C. Liu, Inorg. Chim. Acta 453 (2016) 488–493, https://doi.org/10.1016/j.ica.2016.09.016.
[9] S.S.F. Carvalho, N.M.F. Carvalho, Inorg, Chem. Comm. 108 (2019) 107507, , https://doi.org/10.1016/j.inoche.2019.107507.
[10] J.-M. Hu, R. Guo, Y.-G. Liu, G.-H. Cui, Inorg. Chim. Acta 450 (2016) 418–425, https://doi.org/10.1016/j.ica.2016.06.042.
[11] H. Guo, Z. Yu, Y. Su, X.-D. Jiang, Inorg. Chim. Acta 508 (2020) 119625, , https://doi.org/10.1016/j.ica.2020.119625.
[12] L.-J. Li, L.-K. Yang, Z.-K. Chen, Y.-Y. Huang, B. Fu, J.-L. Du, Inorg. Chem. Comm. 50 (2014) 62–64, https://doi.org/10.1016/j.inoche.2014.10.020.
[13] S. Lu-Lu, Z. Tian-Rui, Z. Li-Ming, L. Ke, L. Bao-Long, W. Bing, Inorg. Chem. Comm. 85 (2017) 16–20, https://doi.org/10.1016/j.inoche.2017.04.028.
[14] Y.-Y. Yang, M.-Q. He, M.-X. Li, Y.-Q. Huang, T. Chi, Z.-X. Wang, Inorg. Chem. Comm. 94 (2018) 5–9, https://doi.org/10.1016/j.inoche.2018.05.026.
[15] L.L. Shi, T.R. Zheng, L.M. Zhu, K. Li, B.L. Li, B. Wu, Inorg. Chem. Commun. 85 (2017) 16–20 https://doi:10.1016/j.inoche.2017.04.028.
[16] Y.P. Wu, D.S. Li, Y.P. Duan, L. Bai, J. Zhao, Inorg. Chem. Commun. 36 (2013) 137–140 https://doi:10.1016/j.inoche.2013.08.039.
[17] J. Li, A.N. Pham, R. Dai, Z. Wang, T.D. Waite, J. Hazard. Mater. 392 (2020) 122261https://doi:10.1016/j.jhazmat.2020.122261.
[18] W. Wu, Z.-D. Luo, J. Wang, J. Liu, Inorg. Chem. Comm. 85 (2017) 2–4, https://doi.org/10.1016/j.inoche.2017.03.025.
[19] Y. Pan, W. Liu, D. Liu, Q. Ding, J. Liu, H. Xu, M. Trivedi, A. Kumar, Inorg. Chem. Comm. 100 (2019) 92–96, https://doi.org/10.1016/j.inoche.2018.12.025.
[20] D.F. Ollis, Front. Chem. 6 (2018) 378 https://doi:10.3389/fchem.2018.00378.
[21] C.B. Liu, H.Y. Sun, X.Y. Li, H.Y. Bai, Y. Cong, A. Ren, G.-B. Che, Inorg. Chem. Commun. 47 (2014) 80–83 https://doi:10.1016/j.inoche.2014.04.034.
[22] N.M.F. Carvalho, A. Horn Jr., O.A.C. Antunes, Appl. Catal. A: Gen. 305 (2006) 140–145 https://doi:10.1016/j.apcata.2006.02.053.
[23] G. C. Silva, N. M. F. Carvalho, A, Horn Jr., E. R. Lachter, O. A. C. Antunes, J. Mol. Catal. A: Chem. 426 (2017) 564–571. http://doi.org/10.1016/j.molcata.2016.08.037.
[24] A.C. Silva, T.L. Fernández, N.M.F. Carvalho, M.H. Herbst, J. Bordinhão, A. Horn Jr, J.L. Wardell, E.G. Oestreicher, O.A.C. Antunes, Appl. Catal. A: Gen. 317 (2007) 154–160, https://doi.org/10.1016/j.apcata.2006.10.012.
[25] N.M.F. Carvalho, A. Horm Jr., A.J. Bortoluzzi, V. Drago, O.A.C. Antunes, Inorg. Chim. Acta 359 (2006) 90–98, https://doi.org/10.1016/j.Ica.2005.07.010.
[26] N.M.F. Carvalho, A. Horn Jr., R.B. Faria, A.J. Bortoluzzi, V. Drago, O.A.C. Antunes, Inorg. Chim. Acta 359 (2006) 4250–4258, https://doi.org/10.1016/j.Ica.2006.06.0121.
[27] M. F. Hossain, Sustainable Development for Mass Urbanization, Elsevier, 2019. https://doi:10.1016/C2018-0-02563-.
[28] N. Niklas, F.W. Heinemann, F. Hampel, T. Clark, R. Alsfasser, Inorg. Chem. 43 (2004) 4663–4673, https://doi.org/10.1021/ic0496774.
[29] K.-Y. Choi, H. Ryu, N.-D. Sung, S. Mancheol, J. Chem. Crystallogr. 33 (2003) 947–950, https://doi.org/10.1023/A:1027485932736.
[30] W.J. Geary, Coord. Chem. Rev. 7 (1971) 81–122, https://doi.org/10.1016/S0010-8545(00)80009-0.
[31] W.L. Driessen, W.L. Groeneveld, F.W. Van der Wey, Recl. Trav. Chim. Pays-Bas 89 (1970) 353–367, https://doi.org/10.1002/recl.19700890403.
[32] J.S. Pap, B. Kripli, I. Bors, D. Bogáth, M. Giorgi, J. Kaizer, G. Speier, J. Inorg. Biochem. 117 (2012) 60–70, https://doi.org/10.1016/j.jinorgbio.2012.08.012.
[33] G.B. Deacon, R.J. Phillips, Coord. Chem. 33 (1980) 227–250, https://doi.org/10.1016/S0010-8545(00)80455-5.
[34] T. Okuno, S. Ohba, Y. Nishida, Polyhedron 16 (1997) 3765–3774, https://doi.org/10.1016/S0277-5387(97)00147-2.
[35] C.-F. Liu, C.-Y. Liu, Z.-G. Ren, J.-P. Lang, Eur. J. Inorg. Chem. (2019) 1816–1824, https://doi.org/10.1002/ejic.201900026.
[36] N.M.F. Carvalho, O.A.C. Antunes, A. Horn, Dalton Trans. (2007) 1023–1027, https://doi.org/10.1039/b616377g.
[37] M. Procner, Ł. Orzeł, G. Stochel, R. Eldik, Eur. J. Inorg. Chem. (2018) 3462–3471, https://doi.org/10.1002/ejic.201800485.